IEEE Access
Multidisciplinary | Rapid Review | Open Access Journal

Received 12 February 2025, accepted 2 March 2025, date of publication 5 March 2025, date of current version 12 March 2025.

Digital Object Identifier 10.1109/ACCESS.2025.3548539

RESEARCH ARTICLE

A Novel High-Sensitivity Time-Domain Fault Classifier Applied to Inverter-Based Resource Interconnection Lines

MOISÉS J. B. B. DAVI[1], MARIO OLESKOVICZ[1], (Member, IEEE), AND FELIPE V. LOPES[2], (Senior Member, IEEE)

[1]Electrical and Computer Engineering Department, University of São Paulo, São Carlos 05508-220, Brazil
[2]Electrical Engineering Department, Federal University of Paraíba, João Pessoa 13566-590, Brazil

Corresponding author: Moisés J. B. B. Davi (moisesdavi@usp.br)

This work was supported in part by the Brazilian Federal Agency for Support and Evaluation of Graduate Education (CAPES), the Sao Paulo Research Foundation (FAPESP), under Grant 2022/00483-0; in part by the National Council for Scientific and Technological Development (CNPq) under Grant 309184/2023-1 and Grant 311547/2021-4; in part by the RCGI–Research Centre for Greenhouse Gas Innovation, hosted by the University of São Paulo (USP), sponsored by FAPESP under Grant 2020/15230-5; in part by TotalEnergies; and in part by Brazil's National Oil, Natural Gas and Biofuels Agency (ANP) through the Research and Development and Innovation (R&DI) Levy Regulation.

ABSTRACT This paper presents a performance review of existing fault classifiers when applied to Inverter-Based Resource (IBR) interconnection lines and proposes a new high-sensitivity time-domain fault classification methodology. The proposed method is based on self-adjusting thresholds, and it is investigated regarding its performance when applied to IBR or conventional generator terminals, being validated for different grid short-circuit levels, various IBR topologies/controls, and considering several fault types, inception angles, resistances, and locations. A typical IBR interconnection system topology is modeled using the PSCAD software for such studies. Comparisons with the main state-of-the-art phase-selection and fault classification methods highlight the superiority of the proposed one that, besides overcoming the challenges presented by IBRs for this task, provides shorter operating times by not relying on phasor estimation techniques.

INDEX TERMS Fault classification, fault classifier, inverter-interfaced resources, phase-selection, renewable energy, wind energy.

NOMENCLATURE

DFIG	Doubly-Fed Induction Generators.
FCG	Full-Converter Generators.
IBRs	Inverter-Based Resources.
IIT-PS	Improved Incremental Torque-based Phase-Selection function.
IT-PS	Incremental Torque-based Phase-Selection function.
$L1$, $L2$	Self-Adjusting Thresholds.
MULT	Grid Short-Circuit Level Multiplier.
NZCA-PS	Negative and Zero sequence Current Angle-based Phase-Selection method.
NZPCA-PS	Negative, Zero, and Positive sequence Current Angle-based Phase-Selection method.
NZPVA-PS	Negative, Zero, and Positive sequence Voltage Angle-based Phase-Selection method.
NZVA-PS	Negative and Zero sequence Voltage Angle-Based Phase-Selection method.
PG	Phase-to-Ground.
PP	Phase-to-Phase.
PPG	Phase-to-Phase-to-Ground.
PPP	Three-Phase.
SCM-C	Superimposed Current Magnitude-based Classifier.
ST	Stockwell Transform.
T1	Type 1 Controls.
T2	Type 2 Controls.

The associate editor coordinating the review of this manuscript and approving it for publication was Mehrdad Saif.

TL	Transmission Line.
V_{maxpp}	Maximum value between $VabM$, $VbcM$, and $VcaM$.
V_{minpp}	Minimum value between $VabM$, $VbcM$, and $VcaM$.
$V0$	Zero sequence voltage.
Va, b, cM	Maximum values of incremental phase voltage energies.
Va, b, c_{EN}	Incremental phase voltage energies.
Va, b, c_{inc}	Incremental phase voltages.
Vab, bc, caM	Maximum values of incremental line voltage energies.
Vab, bc, ca_{EN}	Incremental line voltage energies.
Vab, bc, ca_{inc}	Incremental line voltages.
VM-PS	Voltage Magnitude-based Phase-Selection Function.
VMA-C	Voltage Magnitude and Angle-based Classifier.
WT	Wavelet Transform.

I. INTRODUCTION

Over the years, the increasing penetration of Inverter-Based Resources (IBRs) has been evident. Despite the operational effectiveness of IBRs, such units present challenging scenarios for protection and fault diagnosis schemes due to the atypical behavior of their fault current contributions dictated by inverter control schemes [1]. Thus, this topic has been the focus of various researchers worldwide [2], [3].

Several papers can be found in the literature assessing the IBR impacts on protection systems, including new protection functions [4], [5], new approaches to IBR inverter controls [6], [7], and also recommendations for adjusting existing functions [2], [8], aiming to reduce these impacts. Despite the diversity of papers focused on protecting systems with IBRs, there is still no consensus on the best practices for the phase selection and fault classification tasks in these systems.

In this context, the fault classification and phase-selection methods found in the literature can be divided into: i) fixed decision threshold-based methodologies, ii) artificial intelligence-based proposals, iii) current phasor-based methods, iv) voltage and current phasor-based methods, and v) voltage phasor-based methods.

Regarding fixed decision threshold-based methods, in [9], the authors define an index composed of characteristics extracted from current signals using three different signal processing techniques (Fourier Transform, Hilbert Transform, and Ortonormal Stockwell Transform (ST)), and this index is used to classify faults. In [10], the authors propose similar methodologies that use the Wavelet Transform (WT) detail coefficients of different levels for the current signals of a Transmission Line (TL) terminal. In [11], WT is also employed, and the classification is performed based on subtracting the first-level detail coefficients of both TL terminals. All these methods are based on hard thresholds, which are non-generalizable for decision-making and do not consider IBRs' challenges in their operation. These challenges range from fault contributions dictated by inverter controls [1] to IBR interconnection topologies that tend to attenuate high-frequency transients after the system disturbances [12], [13].

Concerning artificial intelligence-based proposals, in [14], the use of Hyperbolic ST combined with artificial neural networks is proposed to classify faults. Reference [15] presents a fault classification methodology based on WT and support vector machine, using the current signals at one TL terminal. The use of decision trees for fault classification has also been investigated [16]. However, these proposals also do not consider the impacts of the massive integration of IBRs into the power system. References [17], [18], [19], and [20] propose methodologies encompassing the IBR impacts and providing solutions based on machine-learning techniques. Nevertheless, these methodologies depend on the availability of extensive databases of disturbance records for the training and validation processes, which is still an obstacle to their practical application.

Current phasor-based methods represent the most traditional fault classification and phase selection proposals. Such methods include those based on current phase angle information [21], [22] and on the magnitude of these signals [23]. Among the precursors, those based on comparing the superimposed current and fundamental zero sequence phasors can be highlighted [23]. The disadvantage is that they require adjustments of parameters and thresholds for their correct operation, commonly based on analyses of massive databases with disturbance waveforms [23].

Among voltage and current phasor-based methods, those that rely on incremental torques stand out [24]. Improved proposals were applied to systems with IBRs in these methods classes [25]. However, the dependence on adjusting parameters for these techniques to operate should be highlighted, as this also requires analyses of massive databases with disturbance waveforms.

Thus, in an attempt to overcome the challenges posed by IBRs to the methods mentioned above, the literature has presented proposals for fault classification and phase selection based only on voltage phasors, which are less influenced by IBR inverter controls and are more stable for this task. Thus, there are methods based only on voltage phase angle information [26], [27], the magnitude of these signals [4], or both [28], [29]. Despite being presented as promising methods for operation in systems with IBRs, detailed studies evidencing their performance and possible limitations are still scarce. Moreover, a unified performance analysis of fault classifiers, seeking to detail both the challenges that IBRs present to conventional methods and emphasizing the limitations and disadvantages of voltage phasor-based proposals for this task, is also limited.

In addition, works such as [30] and [31], present recent methodologies with operations based on the measurement of voltage and/or current signals for fault classification

in systems with IBRs. However, in [31], the performance limitations of the method proposed in [30] for systems with IBRs are proven. Finally, the method proposed in [31] depends on the definition of fixed thresholds for identifying the ground involvement in faults, following a similar practice to the various other methodologies already mentioned.

Hence, with the literature review, some shortcomings related to fault classification and phase selection tasks in systems with IBRs can be highlighted:

- Conventional methods were designed based on traditional generator fault contribution characteristics, which are significantly modified by IBRs, whose fault contributions are dictated by inverter controls. So, especially the current phasor-based methods face challenges to operate in systems with IBRs;
- Most existing methods are based on the definition of fixed and non-generalizable thresholds, i.e., they require analyses of massive databases with disturbance waveforms to operate reliably;
- Artificial intelligence-based approaches, due to the need for training and testing steps, depend on the availability of data for detailed system modeling/simulation or access to real disturbance records for practical application;
- Although promising voltage phasor-based proposals have been presented for fault classification and phase selection in systems with IBRs, detailed studies showing their performance and possible limitations are scarce.

Based on this context and recognizing the importance of this topic, the main contributions of this paper are:

- A performance review of the main existing fault classification and phase-selection methods is presented, followed by a comparative performance analysis based on realistic case studies, aiming both to highlight and explain the impacts of IBRs on traditional techniques and to emphasize that, although promising, the voltage phasor-based proposals recently presented in the literature include limiting factors in their performance;
- A new high-sensitivity time-domain fault classification method is proposed based on self-adjusting thresholds for its decision-making. Furthermore, since it is a time-domain approach, the phasor estimation process is eliminated, achieving a faster and more stable decision.

This paper is organized as follows. Section II presents the test system and the simulation parameters. Section III discusses the assessed state-of-the-art fault classification and phase-selection methods. Then, Section IV presents a performance analysis of existing fault classification and phase-selection methods. The proposed methodology is detailed and assessed in Section V. Then, Section VI compares the proposed methodology and existing methods in terms of their generalizability for terminals with conventional generators. Finally, the proposed method is evaluated regarding its generalizability to other test systems and noisy signals. Section VII summarizes the main conclusions.

II. TEST SYSTEM

The single-line diagram and parameters of the test system are illustrated in Fig. 1. Aiming to perform evaluations for the main IBR topologies, Full-Converter Generators (FCG) and Doubly-Fed Induction Generators (DFIG) are considered. Regardless of the generator type, the wind power plant is modeled to provide steady-state total active and reactive power outputs of 220.5 MW and 0 var, respectively.

To represent the transmission line, the phase-domain frequency-dependent parameter models provided by PSCAD [32], [33] were employed to ensure the most reliable representation of the parameters and behavior of these components during system disturbances.

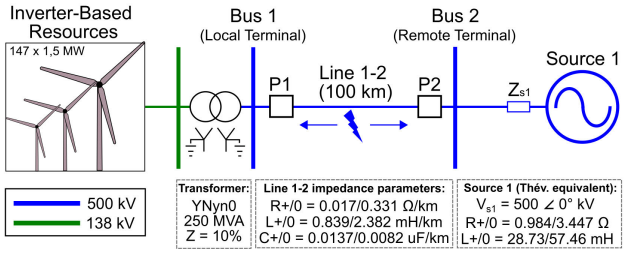

FIGURE 1. Test system single-line diagram.

All controls in the DFIG units are configured as outlined in [34] and [35]. For modeling the FCG, the control settings are adjusted according to the procedures described in [35] and [36].

Aiming to perform evaluations for the main Low Voltage Ride Through (LVRT) requirements, two types of control strategies are considered for the simulations involving FCG. Type 1 Controls (T1) represent the initial strategies relying solely on positive sequence components [37]. In contrast, Type 2 Controls (T2) introduce additional reactive and negative sequence currents following disturbances [7], [37].

A set of fault parameters was defined for the simulations to build a representative database of fault scenarios for the modeled wind power plant. These parameters were based on common variations found in the literature, covering aspects such as fault types, resistances, locations, inception angles, and grid short-circuit levels. Therefore, faults are simulated on Line 1-2, varying its: location (from 0% (P1) to 100% (P2) of Line 1-2 with steps of 10%), inception angle (0, 45, and 90 degrees), type (AG, BG, CG, AB, BC, CA, ABG, BCG, CAG, and ABC), the resistance between phases and ground (R_g of 0, 25, 50, and 100 Ω), and resistance between phases (R_p of 0, 1, 1.5, and 2 Ω).

Moreover, the grid short-circuit level (represented by Source 1 and Z_{s1}) is changed using a multiplier (MULT), meaning how many times the grid short-circuit power is greater than the wind plant-rated power. This MULT varies between 10, 100, and 1000. Thus, considering variations in generator topologies and controls, grid short-circuit levels, and fault parameters, a total of 47,520 scenarios are analyzed.

The measurements at P1 (IBR side) and P2 (grid side) are considered.

III. STATE-OF-THE-ART FAULT CLASSIFICATION AND PHASE-SELECTION METHODS

This section aims to provide details on the fault classification and phase-selection methods evaluated in this paper.

A. NEGATIVE AND ZERO SEQUENCE CURRENT ANGLE-BASED PHASE-SELECTION FUNCTION (NZCA-PS)

The most common current angle-based fault classifiers operate based on symmetrical current components [21], [22].

The decision-making of the NZCA-PS is based on the angular difference between the negative and zero sequence currents, according to the regions shown in Fig. 2. If this difference is within the regions of Fig. 2-(a), the distinction between Phase-to-Ground (PG) and Phase-to-Phase-to-Ground (PPG) faults is based on the smallest range calculated by the PG and Phase-to-Phase (PP) loop mho elements [21], [22]. Meanwhile, if the angular difference falls within the regions of Fig. 2-(b), the distinction between PG and PPG faults is made by the loop with the lowest estimated resistance [21], [22].

Since this method operates based on negative and zero sequence currents, this applies to PG and PPG faults. Moreover, some restrictions for the operation of this method based on the levels of negative ($3|\overrightarrow{I_2}| > 0.25|\overrightarrow{I}_n|$) and zero ($3|\overrightarrow{I_0}| > 0.5|\overrightarrow{I}_n|$) sequence currents, when compared to the nominal current level ($\overrightarrow{I}_n$), are considered [38].

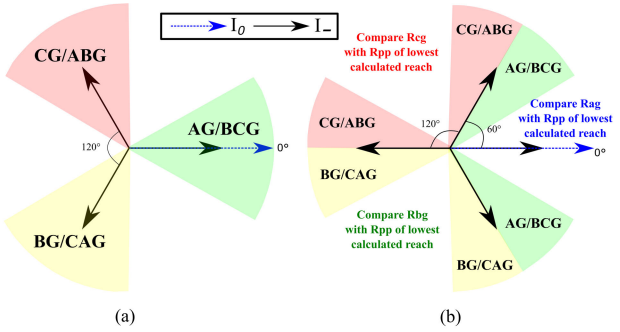

FIGURE 2. Decision-making regions of NZCA-PS.

B. NEGATIVE, ZERO, AND POSITIVE SEQUENCE CURRENT ANGLE-BASED PHASE-SELECTION FUNCTION (NZPCA-PS)

NZPCA-PS's decision-making is based on the angular difference between the negative, zero, and positive sequence currents, according to the regions shown in Fig. 3.

This method operates similarly to the NZCA-PS presented in the previous subsection, including the same restrictions on negative and zero sequence current levels. However, the distinction between PG and PPG faults for NZPCA-PS is based on the angular difference between the negative and positive sequence currents, following the regions illustrated in Fig. 3-(b).

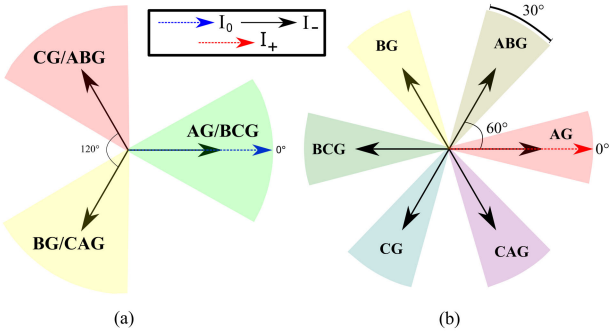

FIGURE 3. Decision-making regions of NZPCA-PS.

TABLE 1. Decision-making rules of SCM-C.

Fault Type	Conditions
AG	$(Is_b < k \cdot Is_a)$ *and* $(Is_c < k \cdot Is_a)$ *and* $(I_0 > I_{min})$
BG	$(Is_a < k \cdot Is_b)$ *and* $(Is_c < k \cdot Is_b)$ *and* $(I_0 > I_{min})$
CG	$(Is_a < k \cdot Is_c)$ *and* $(Is_b < k \cdot Is_c)$ *and* $(I_0 > I_{min})$
AB	$(Is_c < k \cdot Is_a)$ *and* $(Is_c < k \cdot Is_b)$ *and* $(I_0 < I_{min})$
BC	$(Is_a < k \cdot Is_b)$ *and* $(Is_a < k \cdot Is_c)$ *and* $(I_0 < I_{min})$
CA	$(Is_b < k \cdot Is_a)$ *and* $(Is_b < k \cdot Is_c)$ *and* $(I_0 < I_{min})$
ABG	$(Is_c < k \cdot Is_a)$ *and* $(Is_c < k \cdot Is_b)$ *and* $(I_0 > I_{min})$
BCG	$(Is_a < k \cdot Is_b)$ *and* $(Is_a < k \cdot Is_c)$ *and* $(I_0 > I_{min})$
CAG	$(Is_b < k \cdot Is_a)$ *and* $(Is_b < k \cdot Is_c)$ *and* $(I_0 > I_{min})$
ABC	*Else*

C. SUPERIMPOSED CURRENT MAGNITUDE-BASED CLASSIFIER (SCM-C)

The proposal described in [23] is selected to represent the current magnitude-based methods.

The SCM-C can classify all fault types by comparing the magnitude of the superimposed currents (Is_a, Is_b, and Is_c) and the fundamental zero sequence current (I_0). Table 1 illustrates the comparisons conducted for the method's decision-making. Similar to other existing fault classification methods, SCM-C bases its decision on hard thresholds k and I_{min}, which for the evaluations carried out in this paper are 0.3 and 0.1 p.u., respectively, according to [23].

D. INCREMENTAL TORQUE-BASED PHASE-SELECTION FUNCTION (IT-PS)

The IT-PS operates based on three incremental torques [24]:

$$\Delta T_{ab} = Re[\Delta\overrightarrow{V_{ab}} \cdot (1\angle\theta_{L1} \cdot \Delta\overrightarrow{I_{ab}})^*], \quad (1)$$

$$\Delta T_{bc} = Re[\Delta\overrightarrow{V_{bc}} \cdot (1\angle\theta_{L1} \cdot \Delta\overrightarrow{I_{bc}})^*], \quad (2)$$

$$\Delta T_{ca} = Re[\Delta\overrightarrow{V_{ca}} \cdot (1\angle\theta_{L1} \cdot \Delta\overrightarrow{I_{ca}})^*], \quad (3)$$

where $\Delta\overrightarrow{V_{ab}}$, $\Delta\overrightarrow{V_{bc}}$ and $\Delta\overrightarrow{V_{ca}}$ are incremental voltage phasors, $\Delta\overrightarrow{I_{ab}}$, $\Delta\overrightarrow{I_{bc}}$ and $\Delta\overrightarrow{I_{ca}}$ are incremental current phasors, and θ_{L1} is the TL positive sequence impedance angle.

TABLE 2. Decision-making rules of IT-PS.

Fault Type	Conditions
AG	$\Delta T_{ab} > L_{up}$ *and* $\Delta T_{bc} < L_{low}$ *and* $\Delta T_{ca} > L_{up}$
BG	$\Delta T_{ab} > L_{up}$ *and* $\Delta T_{bc} > L_{up}$ *and* $\Delta T_{ca} < L_{low}$
CG	$\Delta T_{ab} < L_{low}$ *and* $\Delta T_{bc} > L_{up}$ *and* $\Delta T_{ca} > L_{up}$
AB / ABG	$\Delta T_{ab} > L_{up}$ *and* $\Delta T_{bc} < L_{int}$ *and* $\Delta T_{ca} < L_{int}$
BC / BCG	$\Delta T_{ab} < L_{int}$ *and* $\Delta T_{bc} > L_{up}$ *and* $\Delta T_{ca} < L_{int}$
CA / CAG	$\Delta T_{ab} < L_{int}$ *and* $\Delta T_{bc} < L_{int}$ *and* $\Delta T_{ca} > L_{up}$
ABC	$\Delta T_{ab} > L_{up}$ *and* $\Delta T_{bc} > L_{up}$ *and* $\Delta T_{ca} > L_{up}$

TABLE 3. Decision-making rules of IIT-PS.

Fault Type	Conditions
AG	$\Delta T_{ab} > L_{up}$ *and* $\Delta T_{bc} < L_{low}$
BG	$\Delta T_{bc} > L_{up}$ *and* $\Delta T_{ca} < L_{low}$
CG	$\Delta T_{ca} > L_{up}$ *and* $\Delta T_{ab} < L_{low}$
AB / ABG	$\Delta T_{ab} > L_{up}$ *and* $L_{int} < \Delta T_{bc} < L_{sup}$
BC / BCG	$\Delta T_{bc} > L_{up}$ *and* $L_{int} < \Delta T_{ca} < L_{sup}$
CA / CAG	$\Delta T_{ca} > L_{up}$ *and* $L_{int} < \Delta T_{ab} < L_{sup}$
ABC	$\Delta T_{ab} > L_{up}$ *and* $\Delta T_{bc} > L_{up}$ *and* $\Delta T_{ca} > L_{up}$

The distinction between the different fault types is made by comparing the values of ΔT_{ab}, ΔT_{bc}, and ΔT_{ca} normalized by the maximum value among them, and the parameters L_{up}, L_{int}, and L_{low}.

Table 2 depicts the rules for determining the fault type using this algorithm, which applies to PG, PP, PPG, and three-phase (PPP) faults but does not differentiate the ground involvement for two-phase faults. For the performance analyses to be conducted in this paper, $L_{up} = 0.7$, $L_{int} = 0.5$, and $L_{low} = 0.35$ are considered [39].

E. IMPROVED IT-PS (IIT-PS)

In [25], modifications are proposed to the IT-PS method to improve performance in systems with IBRs, referred to as the IIT-PS.

This method employs the same incremental torques ΔT_{ab}, ΔT_{bc}, and ΔT_{ca} normalized by the maximum value among them. For the faulty phase selection, the relations shown in Table 3 are assumed for the proposed study [24]. Similarly to IT-PS, IIT-PS also does not indicate the ground involvement or not for two-phase faults. For the studies in this paper, $L_{up} = 0.75$, $L_{int} = 0.25$, and $L_{low} = 0.1$ are employed [25].

F. NEGATIVE AND ZERO SEQUENCE VOLTAGE ANGLE-BASED PHASE-SELECTION FUNCTION (NZVA-PS)

In [27], it is pointed out that the different IBR control types and topologies can challenge methods based on current signals. For this reason, algorithms analogous to NZCA-PS and NZPCA-PS are proposed, using voltage phase angles instead of current phase angles.

Therefore, in this paper, one of these methodologies has been referred to as NZVA-PS. This method uses the same operating principles as the NZCA-PS but employs voltage signals for its decision-making and applies to PG and PPG faults.

It is worth noting that, in [27], operating restriction conditions are not covered for this function as for current signal-based methods. Therefore, such restrictions are not considered for the analyses in this paper.

G. NEGATIVE, ZERO, AND ZERO SEQUENCE VOLTAGE ANGLE-BASED PHASE-SELECTION FUNCTION (NZPVA-PS)

This method uses the same operating principles as the NZPCA-PS but employs voltage signals for its decision-making and applies to PG and PPG faults [27].

H. VOLTAGE MAGNITUDE-BASED PHASE-SELECTION FUNCTION (VM-PS)

In [4], it is emphasized that low fault currents characterize systems with IBRs. Thus, despite all the challenges IBRs present to current-based methods, this characteristic also results in more considerable undervoltages on faulted phases, favoring voltage magnitude-based algorithms.

In this context, Fig. 4 illustrates the schematic of the method referred to in this paper as the VM-PS. This schematic distinguishes between AG and AB/ABG faults, which can also be extended to other asymmetrical fault types. Thus, this method applies to PG, PP, and PPG fault types but does not differentiate the ground involvement for two-phase faults.

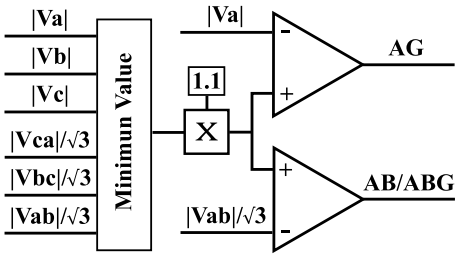

FIGURE 4. Undervoltage faulted-loop selection logic (AG and AB faults) [4].

The VM-PS's decision-making is based on two simple steps:

1) A decision threshold is defined based on the loop voltage with the lowest magnitude (AG, BG, CG, AB, BC, or CA, with the magnitude of the phase-to-phase loop voltages divided by $\sqrt{3}$) multiplied by 1.1;
2) The loop voltage (AG, BG, CG, AB, BC, or CA) with a magnitude lower than the defined threshold is selected, indicating the faulted phases.

I. VOLTAGE MAGNITUDE AND ANGLE-BASED FAULT CLASSIFIER (VMA-C)

The method proposed in [29], referred to in the paper as VMA-C, uses the angular difference between negative and zero sequence voltages, defining three main regions with an angular range of 120°, which indicate AG/BCG, BG/CAG, or CG/ABG faults, as shown in Fig. 5. The fault type is then chosen using the positive, negative, and zero sequence voltage modules, as well as the phase voltage variation

magnitudes (ΔV_A, ΔV_B, and ΔV_C), calculated by $\Delta V_\Phi = |V_\Phi| - |V_{\Phi-nominal}|$, where Φ represents the phases A, B, or C.

Fig. 6 illustrates the schematic for distinguishing between ABC, AG, AB, and ABG faults. This schematic can also be extended to other fault types [29]. Thus, the method applies to all fault types.

IV. PERFORMANCE ANALYSIS OF EXISTING FAULT CLASSIFICATION AND PHASE-SELECTION METHODS

For the discussions of this section, the state-of-the-art methods are evaluated for the database of 47,520 scenarios obtained with the test system, focusing on measurements on the IBR side (point P1). For preliminary assessments, the methods' response is assumed to be 100 ms after the fault inception, eliminating influences from the phasor estimation algorithm's stabilization process and the IBR controls' response time. For techniques based on incremental quantities, these quantities are calculated by subtracting the actual sample from the sample taken ten cycles earlier.

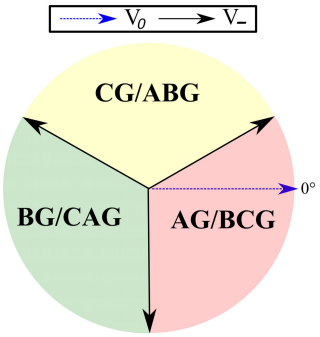

FIGURE 5. Decision-making regions of VMA-C [29].

Subsequently, the methods' response in time is also evaluated to highlight how the phasor estimation process and the IBR control response influence the strategies and their operating times.

A. PRELIMINARY PERFORMANCE ANALYSIS

The success rates, by method, obtained in the preliminary analyses are shown in Fig. 7. Success rates were calculated by dividing the number of fault scenarios in which the fault classification or phase selection was performed correctly by the total number of scenarios assessed. It is worth noting that some fault types were disregarded for some methods since these are not applicable. For example, for the NZCA-PS and NZPCA-PS methods, which only operate for PG and PPG faults, PP and PPP fault scenarios were disregarded in the accuracy calculation. Therefore, the aim is to analyze the methods' accuracy while complying with their operational limitations.

Regarding the current angle-based methods (NZCA-PS and NZPCA-PS), the suppression of the negative sequence component that characterizes FCG-T1 has prevented correct operations by these methods for this generator type since the

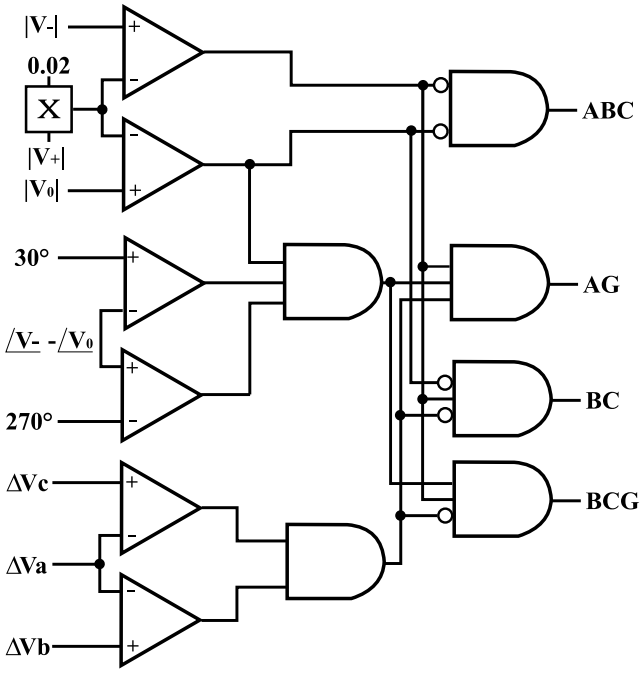

FIGURE 6. Operational schematic of VMA-C [29].

provided negative sequence current levels were insufficient to reach the operating restriction threshold. For DFIG and FCG-T2, in contrast, significantly higher success rates were observed for NZCA-PS and low percentages for NZPCA-PS.

Concerning the NZCA-PS method, success rates were higher than 91.7% for DFIG and lower than 75.6% for FCG-T2. The lower success rates for the NZCA-PS method for FCG-T2 are related to the injection of synthetic negative sequence currents by this IBR type, with values proportional to the negative sequence voltages. Thus, for scenarios with high fault resistances, i.e., scenarios in which the negative sequence voltages have low magnitudes, a low negative sequence current is injected, which can be insufficient to trigger the adjusted restriction threshold. To justify these occurrences, Fig. 8 illustrates how the levels of negative sequence currents, in p.u., vary according to the fault resistance increase. This figure considers the application of AG faults at 70% of TL 1-2, with a 90° inception angle. It can be seen that increasing the fault resistance results in a more abrupt reduction in the negative sequence currents supplied by the FCG-T2 when compared to DFIG. This reduction is influenced by the curve that defines this negative sequence current supply. Furthermore, the NZCA-PS restriction threshold choice will also affect this method's operation.

Regarding the method used to distinguish between PG and PPG faults, the strategy used by NZCA-PS proved to be more promising since the NZPCA-PS method uses the phase angle of the positive sequence current, which, as already discussed in other papers in the literature [40], tends to be strongly influenced by the IBR control characteristics.

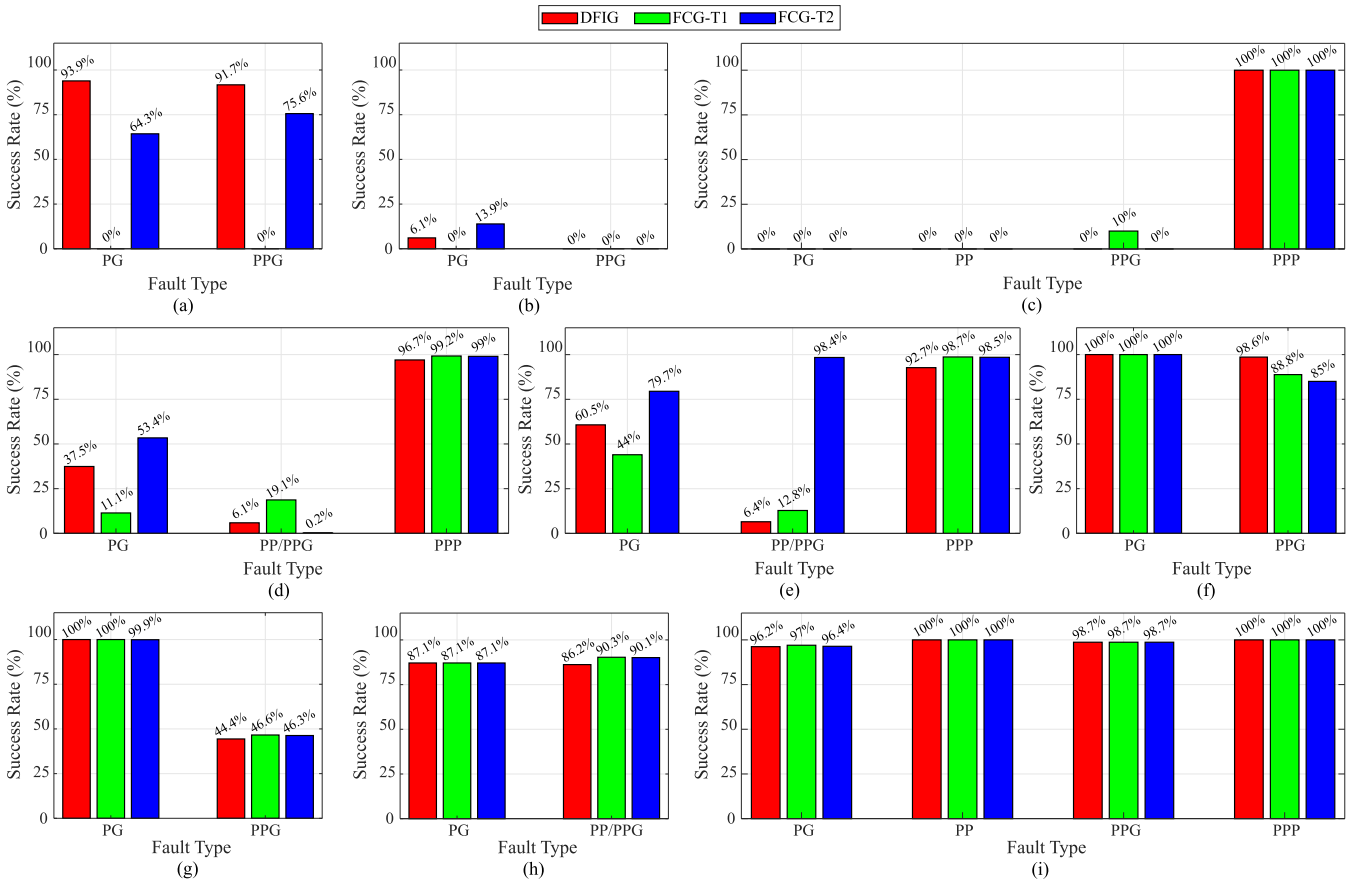

FIGURE 7. Success rates of (a) NZCA-PS, (b) NZPCA-PS, (c) SCM-C, (d) IT-PS, (e) IIT-PS, (f) NZVA-PS, (g) NZPVA-PS, (h) VM-PS, and (i) VMA-C methods, considering measurements at P1 (IBR side).

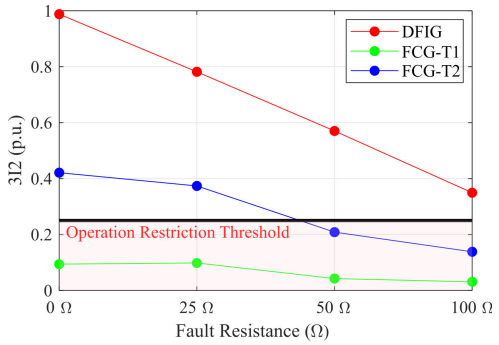

FIGURE 8. Behavior of the negative sequence current magnitude supplied in an AG fault scenario at 70% of TL, with 90° inception angle, and assuming fault resistance variation.

Considering the SCM-C, which operates based on the variation in current levels, good performance was achieved only for three-phase faults since balanced three-phase current contributions are expected for this fault type, regardless of the generator connected to the system. The method returned very low success rates for the other fault types, showing that in systems with IBRs, current magnitudes are not promising features for the fault classification task. Two main points can explain this condition: a) for faults with ground involvement, the measurements at P1 have strong characteristics of the dominant zero sequence current coming from the grid (in this paper represented by conventional generators), as shown in Fig. 9; b) for two-phase faults, the modulation characteristics of the supplied negative sequence current and the limitation of the inverter output currents result in current waveforms with unconventional characteristics, as shown in Fig. 10. Therefore, the operational behavior of IBR proves to be challenging for current magnitude-based fault classification algorithms, except for three-phase fault conditions where a balanced three-phase profile is expected.

About the IT-PS and IIT-PS algorithms, with operation based on incremental torques, it is noted that the proposed improvement to the IIT-PS method was effective, especially for FCG-T2. However, the obtained results are not satisfactory overall. This condition is justified because these methods are also influenced by the measured current magnitudes, which, as previously shown, are strongly influenced by the IBRs.

In contrast, higher success rates were obtained for the voltage signal-based methods, showing that for systems with IBRs, the voltage signals are more suitable and have been

presented as a trend by commercial relay manufacturers for fault classification purposes [27].

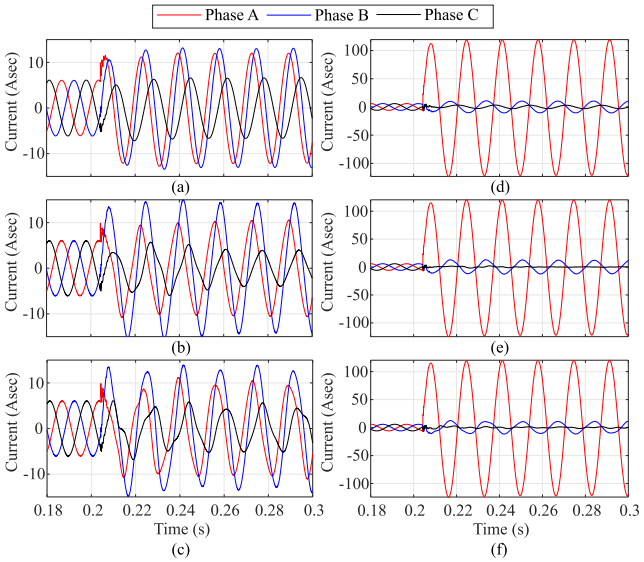

FIGURE 9. Current waveforms measured at points P1 ((a) DFIG, (b) FCG-T1, and (c) FCG-T2) and P2 ((d) DFIG, (e) FCG-T1, and (f) FCG-T2) for an AG bolted fault at 50% of TL, and a 90° inception angle.

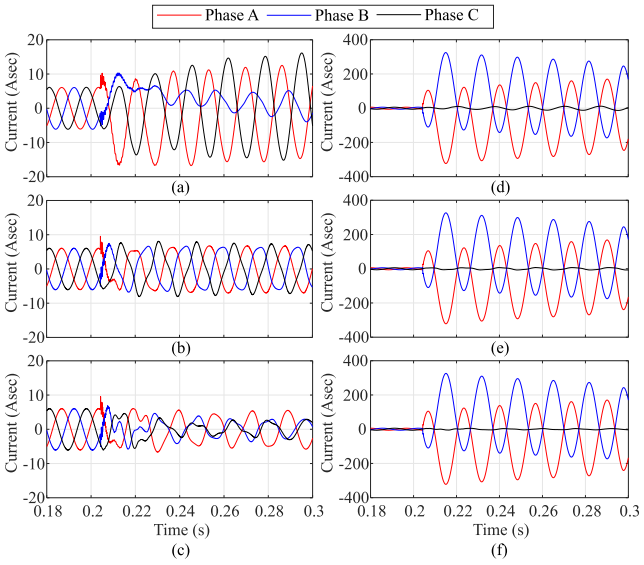

FIGURE 10. Current waveforms measured at points P1 ((a) DFIG, (b) FCG-T1, and (c) FCG-T2) and P2 ((d) DFIG, (e) FCG-T1, and (f) FCG-T2) for an AB bolted fault at 50% of TL, and a 90° inception angle.

The voltage angle-based methods (NZVA-PS and NZPVA-PS) proved very reliable, although only applied to PG and PPG faults. Incorrect operations were observed for PPG faults involving high resistances, which is justified by the impact of this fault resistance on the phase angle difference between the zero and negative sequence voltages. This impact is proved in Fig. 11, illustrating the phase angle difference with increasing resistance for an ABG fault at 70% of TL 1-2, with a 0° inception angle.

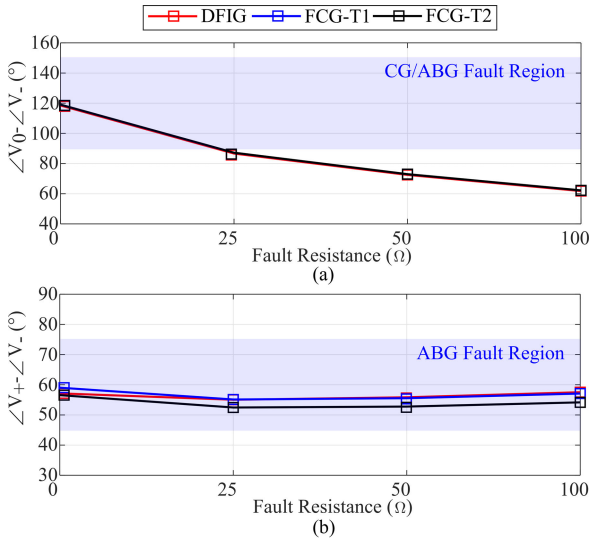

FIGURE 11. The behavior of the angular difference between (a) zero and negative, and (b) positive and negative sequence voltages for ABG faults at 70% of TL, with a 0° inception angle, and assuming fault resistance variation.

Although the fault resistance directly impacts the angular difference between zero and negative sequence voltages, it does not significantly affect the angular difference between positive and negative sequence voltages for PPG faults. However, it can be seen that the NZPVA-PS algorithm obtained lower success rates than NZVA-PS. This condition is justified because NZVA-PS expands the regions of Fig. 2-(a) by a further 60° in Fig. 2-(b), accommodating more significant variations for the angular difference between the zero and negative sequence voltages. In other words, if the NZPCA-PS method expanded each of the three decision regions in Fig. 3-(a) by ±60° while maintaining confirmation of the fault type based on the regions of Fig. 3-(b), the performance of this phase selection algorithm would be improved. New tests were carried out for this condition, and it was observed that the success rates for PPG faults increased from 44.4%, 46.6%, and 46.3% to 91.5%, 93.9%, and 92.6% considering DFIG, FCG-T1, and FCG-T2, respectively. Nevertheless, these methods tend to operate incorrectly for even higher fault resistances.

The VM-PS achieved success rates of more than 86% for the analyzed scenarios, making it a simple and practical option for classifying faults in systems with IBRs. However, as the grid short-circuit level and the fault resistances increase, this method tends to operate incorrectly due to slight variations in the voltage magnitudes. Fig. 12 proves these conditions for an AG fault with 100 Ω, applied at 70% of TL, with 0° inception angle, and assuming the variation of the grid short-circuit level (MULT).

Finally, the VMA-C method uses a strategy similar to the expansion of regions mentioned in the discussions on the NZVA-PS and NZPVA-PS methods, as shown in Fig. 5, including decisions based on the magnitude of negative,

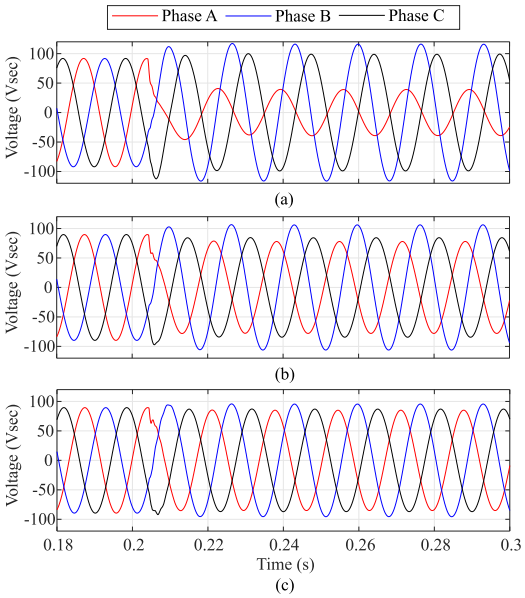

FIGURE 12. Voltage waveforms measured at point P1, for AG faults at 70% of TL, with 90° inception angle, and 100 Ω resistance, assuming the MULT parameter of (a) 10, (b) 100, and (c) 1000.

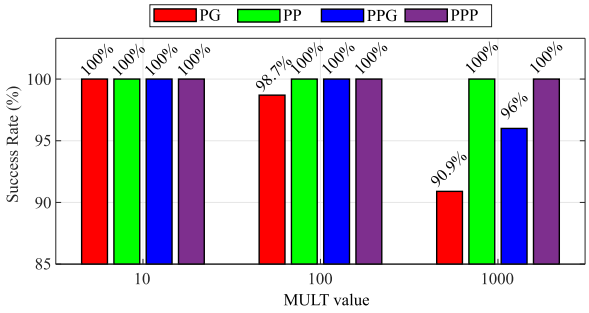

FIGURE 13. Performance of the VMA-C method, assuming variation of the MULT parameter between 10, 100, and 1000.

positive, and zero sequence voltages, as well as incremental voltages (ΔV_A, ΔV_B, and ΔV_C) to enable the classification of all fault types. As discussed in the previous paragraphs, the voltage signal magnitudes and angles offer promising conditions for classifying faults in systems with IBRs, which makes the VMA-C method the most complete and adequate option among the evaluated state-of-the-art approaches. However, this method also tends to be impacted by an increase in the grid's short circuit level and fault resistances. This condition can be noticed in Fig. 13, which shows the percentage of correct operations for the VMA-C method by fault type as the MULT parameter increases. In other words, as the grid strength to which the IBR is connected increases, the method tends to fail for PG and PPG faults with higher resistances.

In summary, it is important to emphasize that the aforementioned misjudgment situations enabled some important conclusions regarding the need for adaptations and improvements in fault classification methods to be applied successfully in systems with IBRs. Among these conclusions, the following stand out:

- Current signals should be avoided in decision-making related to fault classification or phase selection since both the magnitude and phase angle are severely impacted by the IBR control strategies;
- Although voltage signals proved to be more promising for the fault classification task, it was noted that the behavior of the angular difference between the zero and negative sequence voltages as the fault resistance increased led to incorrect operations and that this quantity should be avoided for classifiers' decision-making;
- For grids with a high short-circuit level and fault scenarios with high resistances, the variations in voltage signal magnitude were very slight, despite transient variations occurring after the fault inception. Therefore, under these conditions, voltage phasor magnitude-based decision-making stages should be avoided.

B. RESPONSE IN TIME PERFORMANCE ANALYSIS

This section evaluates the classifiers' response in time to demonstrate their stability and response time characteristics. For the analysis, only the voltage signal-based methods (NZVA-PS, NZPVA-PS, VM-PS, and VMA-C) are considered, which have proved to be the most promising for the fault classification task in systems with IBRs.

The tests considered AG, AB, ABG, and ABC faults at 70% of TL 1-2, assuming MULT equals 10. Fig. 14 illustrates the methods' responses for bolted faults with 0° inception angle. Fig. 15 illustrates these responses for faults with 100 Ω resistances and 90° inception angle. Regarding the evaluated IBR topology, as no significant influences were observed for the three IBR types (see Fig. 7), the results consider FCG-T2.

The results for NZVA-PS and NZPVA-PS indicate operating times of up to 6 ms for AG faults and 43 ms for ABG faults. The scenario with higher fault resistance caused both an impact on the stability of the NZVA-PS, resulting in more extended periods for the method to provide a stable response, and incorrect operation of the NZPVA-PS method due to the non-extension of the decision regions of Fig. 3-(a). These conditions are justified by the variation in the angular difference between the zero and negative sequence voltages for faults with higher resistances, shown in Fig. 11-(a).

For the VM-PS, the classification of two-phase faults was successful for both evaluated scenarios, with operating times of up to 41 ms for ABG faults and 18 ms for AB faults. Operating times of less than 5 ms were observed for bolted AG fault scenarios and incorrect operations for faults with higher resistance. The discussions about Fig. 12 justify these conditions, showing the impact of fault resistance and grid strength on the fault voltage magnitudes.

Finally, the VMA-C method successfully classified all the fault types for both scenarios. The operating times were up to 14, 11, 14, and 35 ms for AG, AB, ABG, and ABC faults,

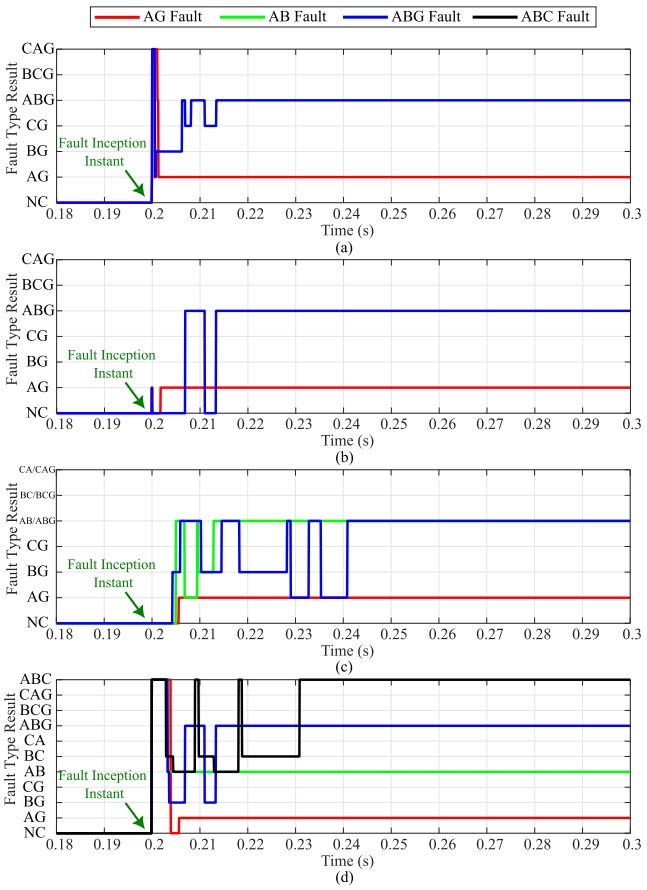

FIGURE 14. Response in time of (a) NZVA-PS, (b) NZPVA-PS, (c) VM-PS, and (d) VMA-C methods for bolted faults at 70% of TL, with 0° inception angle, and MULT of 100.

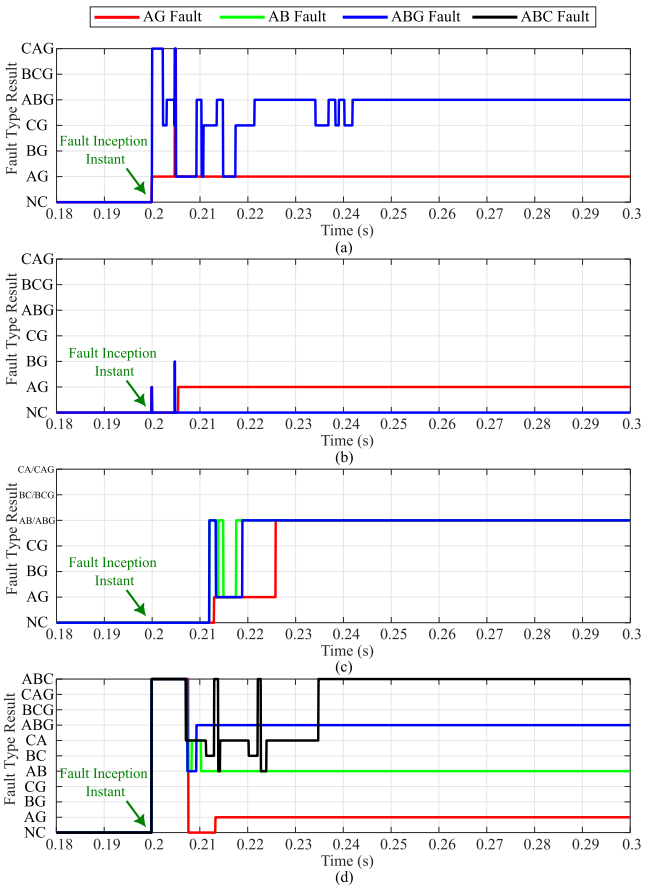

FIGURE 15. Response in time of (a) NZVA-PS, (b) NZPVA-PS, (c) VM-PS, and (d) VMA-C methods for faults at 70% of TL, with 90° inception angles, resistance of 100 Ω, and MULT of 100.

respectively, with a significant response time observed for three-phase faults.

The discussions above show that even though voltage signals are less influenced by IBRs and more suitable for the fault classification task in systems with these generator topologies, factors such as the dependence on the phasor estimation process can result in delays in the assessed methods' response time and incorrect results depending on the selected method and considered fault parameters.

V. PROPOSED FAULT CLASSIFICATION/PHASE-SELECTION METHOD

Once a case study-based review of the main state-of-the-art fault classifiers' performance has been conducted, it is noted that voltage signals have promising characteristics for the fault classification task in systems with IBRs. Therefore, the method to be presented uses these signals, with the additional contribution of dispensing the phasor estimation stage that results in increased response times for the methodologies. To do so, the method is based on the variations experienced by the time-domain voltages after fast transients caused by disturbances.

Furthermore, relying on time-domain quantities increases the sensitivity and robustness of the proposed method since even for scenarios with high fault resistances and stronger grids, there are more pronounced transients in the faulty phases, as shown in Fig. 12-(c). In other words, this methodology can provide assertiveness for the fault classification task, even in scenarios where state-of-the-art methods fail.

The operation of the proposed methodology starts with a few stages that calculate certain quantities used in its decision-making process. These stages are described below:

1) Acquisition of additional samples for 1/4 cycle after fault detection. The selection of a 1/4 cycle acquisition time after the fault was based on a comprehensive analysis of the transient behavior of voltage signals conducted across an extensive and diverse fault scenario database. This analysis revealed that this time interval balances speed and accuracy, thus meeting the expected performance criteria under various operating conditions. This choice also minimizes misclassifications while ensuring the fastest and most precise fault classification response. In addition, the voltage signal

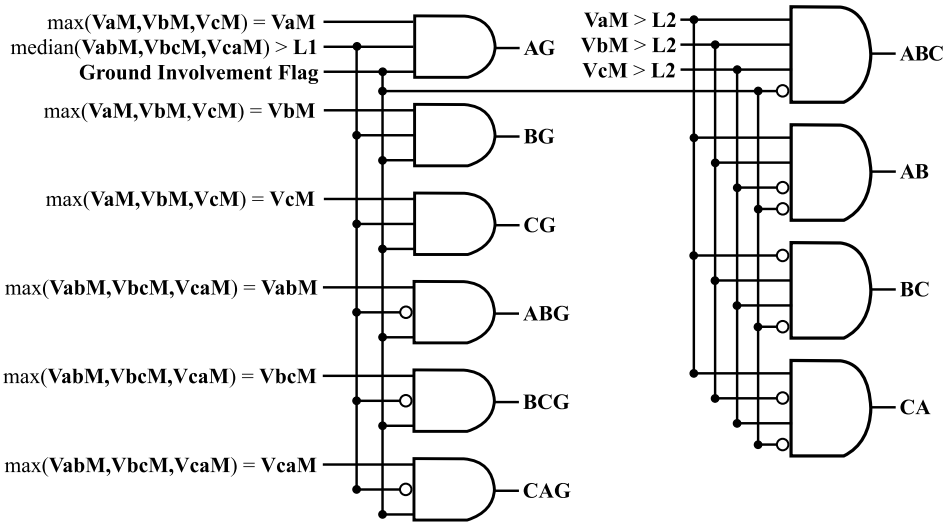

FIGURE 16. Schematic showing the proposed fault classification method stages.

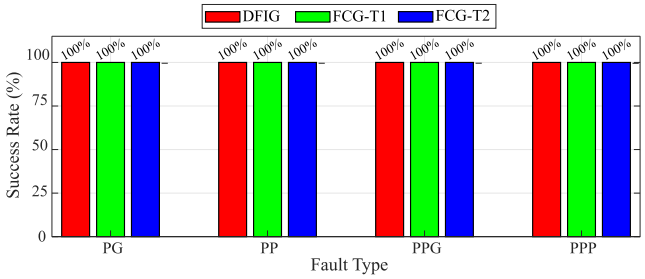

FIGURE 17. Success rates of the proposed method.

buffers must include at least two pre-fault cycles to calculate incremental quantities;

2) Calculation of incremental phase (Va_{inc}, Vb_{inc}, and Vc_{inc}) and line (Vab_{inc}, Vbc_{inc}, and Vca_{inc}) voltages, by:

$$V_{inc}(i) = V(i) - V(i-N), \tag{4}$$

where V represents the signal under analysis, i is the index of the current sample, and N is the number of points per cycle of the signal under analysis. In this stage, the zero sequence voltage ($3V0$) is also calculated using:

$$3V0 = Va + Vb + Vc, \tag{5}$$

where Va, Vb, and Vc represent the instantaneous values of phase A, B, and C voltage signals, respectively;

3) Energy calculation of the incremental voltages (Va_{EN}, Vb_{EN}, Vc_{EN}, Vab_{EN}, Vbc_{EN}, Vca_{EN}) considering a sample window J with N samples (N proportional to 1/16 cycle) and shift at each sample, by:

$$EN = \sum_{i=1}^{N} |J[i]^2|. \tag{6}$$

So, the maximum values for each calculated signal energy are found (VaM, VbM, VcM, $VabM$, $VbcM$, $VcaM$). The choice of incremental voltages, as well as the calculation of the energy of these signals, aims to make the method more sensitive to the transient variations experienced by the system voltages after the fault inception;

4) Definition of the self-adjusting threshold ($L1$ and $L2$) based on the phase voltages' energy:

$$L1 = \frac{V_{maxpp} + V_{minpp}}{2} \tag{7}$$

$$L2 = (1/3) \cdot max(\frac{Va_{inc} + Vb_{inc} + Vc_{inc}}{3}) \tag{8}$$

where V_{maxpp} and V_{minpp} are the maximum and minimum values, respectively, between $VabM$, $VbcM$, and $VcaM$. Note that $L1$ and $L2$ are based on the incremental phase voltage energy values, i.e., the method is free of fixed thresholds;

5) Identifying ground involvement (Ground Involvement Flat = 1) or not (Ground Involvement Flat = 0) in the fault, checking whether the maximum absolute value of $3V0$ exceeds 1% of the rated voltage increased by the maximum value of $|3V0|$ obtained in the two-cycle pre-fault window. Using the maximum $|3V0|$ value in the pre-fault window is intended to make the decision robust even in systems with unbalanced or noisy signals. In turn, the 1% of the rated voltage aims to provide a variable safety margin for identifying ground involvement.

Once these calculation stages have been completed, the obtained quantities and thresholds are applied to the schematic illustrated in Fig. 16 to provide the final response by the method, specifying the fault type.

The definition of the equations for $L1$ and $L2$ thresholds was based on a massive analysis of voltage signal transient

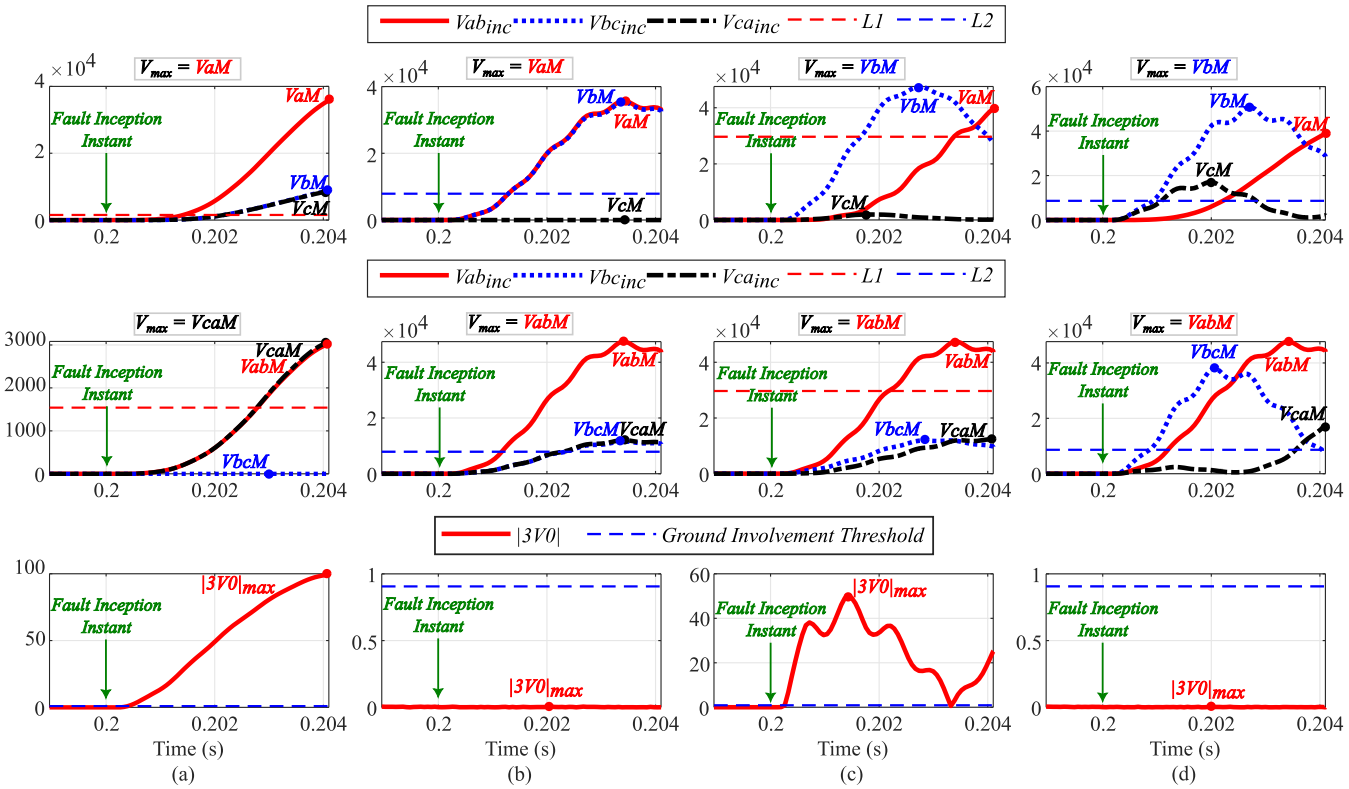

FIGURE 18. Decision-making quantities of the proposed method, considering (a) AG, (b) AB, (c) ABG, and (d) ABC faults applied at 50% of TL with 0° inception angle, assuming MULT = 100 and DFIG.

behavior for diverse fault scenarios. For PG faults, for instance, it was verified that the median between the values *VabM*, *VbcM*, and *VcaM* was, in most cases, close to the maximum value among these signals, while for PPG faults, it was close to the minimum value. Therefore, to determine a reliable value for distinguishing between PG and PPG faults, the $L1$ equation was defined as the average of the maximum and minimum values between *VabM*, *VbcM*, and *VcaM*. For PPP faults, it was noted that the signals *VaM*, *VbM*, and *VcM* returned similar values. Conversely, for PP faults, the non-faulted phase returned much lower values than the others for the *VaM*, *VbM*, and *VcM* signals. Moreover, the maximum value obtained from the average of incremental voltages (Va_{inc}, Vb_{inc}, and Vc_{inc}) looked similar to *VaM*, *VbM*, and *VcM* values for PPP faults. Therefore, it was determined for the L2 equation that this maximum value divided by three would be a promising indicator for PPP faults when exceeded by *VaM*, *VbM*, and *VcM* simultaneously.

When assessing the performance of the proposed method, success rates shown in Fig. 17 are achieved, considering the 47,520 scenarios initially outlined. These results show that the proposed fault classification methodology outperforms state-of-the-art methods (success rates shown in Fig. 7) and has a response time limited to 1/4 cycle plus the decision-making time, which tends to be very short and varies according to the processor used.

Fig. 18 exemplifies the variations in the processed signal energies, as well as the quantities used for decision-making in the proposed method for AG (Fig. 18-(a)), AB (Fig. 18-(b)), ABG (Fig. 18-(c)), and ABC (Fig. 18-(d)) faults. This example represents bolted faults, applied at 50% of TL with 0° inception angle, assuming MULT = 100 and DFIG. Fig. 18 highlights both the self-adjusting capacity of L1 and L2 thresholds and the suitability of the proposed threshold for verifying the ground's involvement in faults.

Moreover, Fig. 19 illustrates the phase voltage energies for AG faults at 50% of TL with 0° inception angle, varying the fault resistance between 25, 50, and 100 Ω, MULT = 10 and 1000, and DFIG. The results show that although the magnitudes of the energies are affected, the relationships between them used for the method's decision-making are not significantly impacted. Thus, the technique maintains assertiveness in fault classification even for higher-resistance scenarios and stronger grids. Moreover, the relationships for the line voltage energies were also unaffected, and the maximum value of $|3V0|$ was significantly higher than the self-adjusted threshold.

Finally, Fig. 20 shows the decision-making quantities for AG faults at 50% of TL with 25 Ω of resistance, varying the inception angle between 0°, 45°, and 90°, MULT = 10 and 1000, and DFIG. These results demonstrate that variations in the fault's inception angles do not affect the proposed method's performance. For the scenarios shown in Fig. 20,

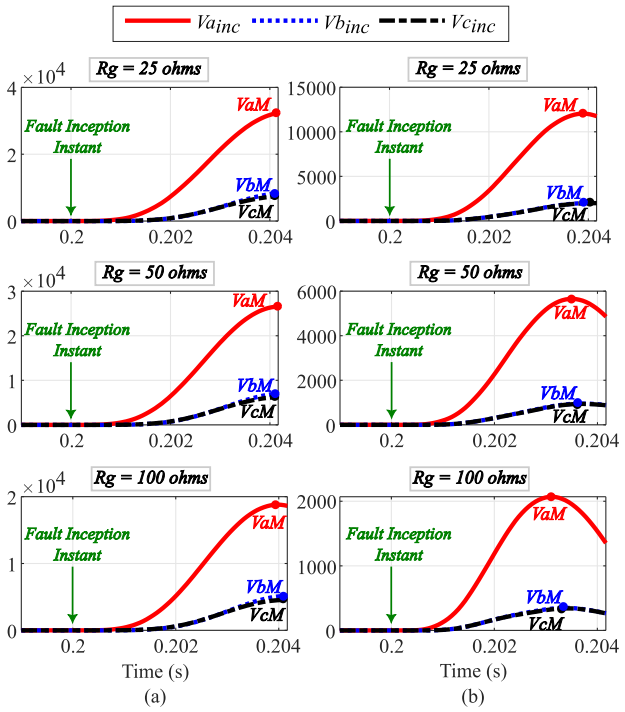

FIGURE 19. Decision-making quantities of the proposed method, considering AG faults at 50% of TL with 0° inception angle, varying the fault resistance between 25, 50, and 100 Ω, and MULT = (a) 10 and (b) 1000.

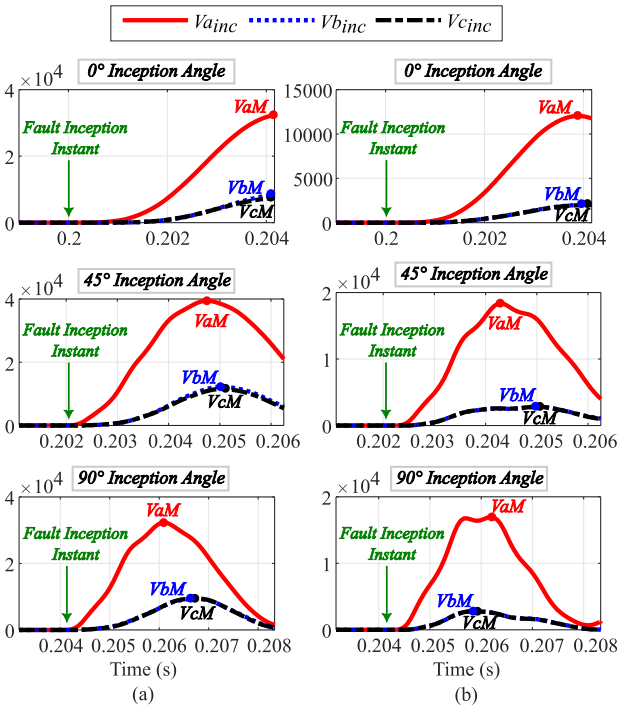

FIGURE 20. Decision-making quantities of the proposed method, considering AG faults at 50% of TL with 25 Ω of resistance, varying the inception angle between 0°, 45°, and 90°, and MULT = (a) 10 and (b) 1000.

the relationships for the line voltage energies were unaffected, and $|3V0|$ exceeded the self-adjusted threshold.

VI. FAULT CLASSIFIERS GENERALIZABILITY FOR TERMINALS WITH CONVENTIONAL GENERATORS

This section evaluates the classifiers' performances with measurements from the grid side (point P2), aiming to explore the methods' generalizability for terminals with conventional generators. The same 47,520 scenarios are employed for the evaluations. Fig. 21 shows the success rates obtained by each method.

Some findings are highlighted about these results:

- The current signal-based methods (NZCA-PS, NZPCA-PS, and SCM-C) performed significantly better compared to the results in Fig. 7, with NZCA-PS maintaining its superiority. This improvement in performance is expected, given that these methods were designed based on the behavior of conventional generator fault currents;
- The incremental torque-based methods (IT-PS and IIT-PS) also experienced increased success rates. The IT-PS results were superior to IIT-PS for asymmetrical faults. This is expected given that IIT-PS includes modifications in its decision-making to accommodate the atypical characteristics of IBR fault contributions;
- The NZVA-PS and NZPVA-PS methods maintained satisfactory performance, and NZVA-PS continued to be superior. It is worth noting that these methods are only applied to PG and PPG faults;
- The VM-PS, based exclusively on the voltage magnitudes, experienced reduced success rates, and this is expected, given that its application is favored only for weak source terminals (IBRs);
- VMA-C also experienced significant drops in the success percentages, especially for PG and PPG faults. In other words, even though it was the best proposal among the evaluated state-of-the-art methods, its generalization capacity for applications in conventional generator terminals is not satisfactory;
- Finally, the proposed method remained the best-performing among all the methods, not only because it applies to all fault types but also because it returned the highest success rates for the evaluated scenarios. This validates the generalizability of this method also for conventional generator terminals.

Table 4 summarizes all the classifiers' average success rates, considering all fault types. Therefore, it can be concluded that state-of-the-art methods designed to overcome the challenges resulting from the massive integration of IBRs in the system do not present satisfactory generalizability when applied to terminals with conventional generators. In this context, the proposed method stands out mainly for:

- Its applicability to all fault types: As observed from the different fault classification and phase-selection methods discussed, some do not apply to all fault types. The proposed method, in contrast, besides presenting the best performance, can be applied to all fault types;

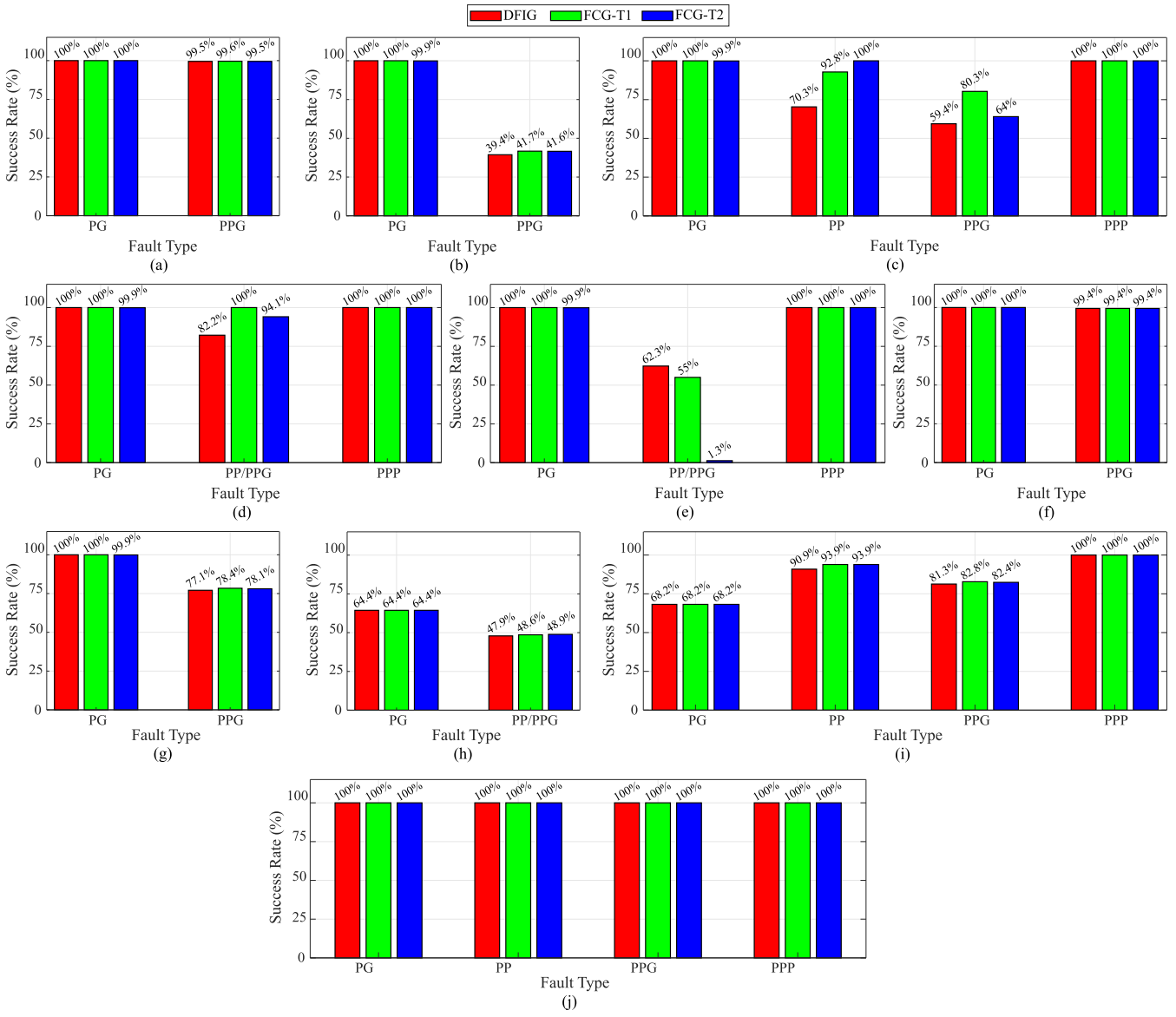

FIGURE 21. Success rates of (a) NZCA-PS, (b) NZPCA-PS, (c) SCM-C, (d) IT-PS, (e) IIT-PS, (f) NZVA-PS, (g) NZPVA-PS, (h) VM-PS, (i) VMA-C, and (j) proposed methods, considering measurements at P2 (grid side).

- Its short time response: The results in Section IV-B show that the methods based on phasor estimation, which represent a significant portion of the existing proposals in the literature, have response time delays of up to 35 ms, depending on the fault type and severity. The proposed method, on the other hand, operates in the time domain and has response times limited to $\frac{1}{4}$ of a cycle added to the decision-making time, which tends to be very short and varies according to the processor used;
- Its suitability for application in IBR or conventional generators: As demonstrated in Section VI analyses, existing methods that perform better for IBR terminals tend to be negatively impacted when applied to conventional generators. The proposed method, in turn, maintains its high performance regardless of the predominant generation type in the system.

VII. THE PROPOSED METHOD'S GENERALIZABILITY TO OTHER SYSTEMS AND NOISY SIGNALS

A second test system was also evaluated to explore the proposed fault classification methodology's ability to be applied to other systems, and the influence of signal noise on its performance. The single-line diagram and parameters of the second test system are illustrated in Fig. 22 and Table 5, respectively.

This is a sub-transmission system comprising four main 69 kV busbars. The wind farm consists of eight turbines of 1.5 MVA each, connected to the 34.5 kV system by Dyn11 transformers with a 34.5-0.575 kV voltage, 1.75 MVA power,

TABLE 4. Overview of the evaluated methods' average success rate for all fault types.

Method	Average Success Rate for DFIG (meas. at IBR side)	Average Success Rate for FCG-T1 (meas. at IBR side)	Average Success Rate for FCG-T2 (meas. at IBR side)	Average Success Rate for DFIG (meas. at grid side)	Average Success Rate for FCG-T1 (meas. at grid side)	Average Success Rate for FCG-T2 (meas. at grid side)	For which fault classes is the method applicable?
NZCA-PS	92.8%	0.0%	69.9%	99.8%	99.8%	99.8%	PG-PPG
NZPCA-PS	3.0%	0.0%	6.9%	69.7%	70.9%	70.8%	PG-PPG
SCM-C	10.0%	13.0%	10.0%	78.9%	91.9%	89.2%	PG-PP-PPG-PPP
IT-PS	22.7%	24.7%	26.0%	89.3%	100%	96.4%	PG-PP/PPG-PPP
IIT-PS	31.2%	30.7%	92.8%	77.4%	73.0%	40.8%	PG-PP/PPG-PPP
NZVA-PS	99.3%	94.4%	92.5%	99.7%	99.7%	99.7%	PG-PPG
NZPVA-PS	72.2%	73.3%	73.1%	88.6%	89.2%	89.0%	PG-PPG
VM-C	86.5%	89.2%	89.1%	53.4%	53.9%	54.1%	PG-PP/PPG
VMA-C	98.4%	98.7%	98.5%	82.1%	83.5%	83.4%	PG-PP-PPG-PPP
Proposed Method	**100%**	**100%**	**100%**	**100%**	**100%**	**100%**	**PG-PP-PPG-PPP**

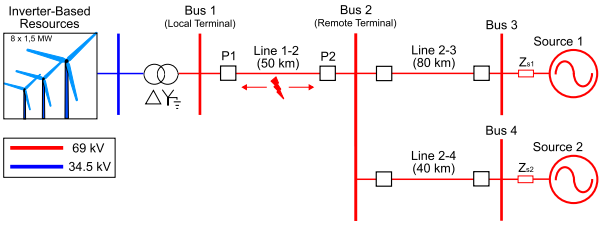

FIGURE 22. New test system single-line diagram.

TABLE 5. New test system parameters.

Parameters	Values
Source 1	V_{s1} = 71,76 ∠ 0° kV R+/0 = 0,112 / 0,435 Ω L+/0 = 16,976 / 48,805 mH
Source 2	V_{s2} = 70,38 ∠ -25° kV R+/0 = 0,431 / 1,678 Ω L+/0 = 65,507 / 188,330 mH
Transformer YNd1 (69 - 34,5 kV)	14 MVA - Z = 10%
Transmission Lines	R+/0 = 0,159 / 0,516 Ω/km L+/0 = 1,327 / 3,929 mH/km C+/0 = 0,00877 / 0,00596 μF/km

and 6% impedance. Transmission lines of 50, 80, and 40 km connect busbars 1-2, 2-3 and 2-4, respectively. On busbars 3 and 4, sources were inserted in series with impedances for the equivalent representation of the power grid. The active and reactive powers supplied to the grid by the IBRs were maintained at 12 MW and 0 VAr, respectively, and the measurements at P1 (IBR side) and P2 (grid side) were considered.

DFIG, FCG-T1, and FCG-T2 type IBRs were considered for the wind farm. Therefore, faults were simulated on Line 1-2, varying fault type (AG, BG, CG, AB, BC, AC, ABG, BCG, CAG, and ABC), phase-to-phase resistance (0, 1, 1.5, and 2 Ω), phase-to-ground resistance (0, 25, 50, and 100 Ω), inception angle (0°, 45, and 90°), and location (from 0% to 100% of Line 1-2 with a step of 10%, with 0% being P1). Moreover, besides considering the pure signals obtained from the simulations, these signals were also conditioned to 48 dB noise. Thus, considering the different IBR controls, fault parameters and signal noise levels, 31,680 additional scenarios were simulated and assessed.

TABLE 6. Performance of the proposed method for the new test system, considering measurements at P1 and P2.

Measurement Point	Success Rate (No Noise)	Success Rate (48 dB)
P1 (IBR side)	99.6%	99.6%
P2 (grid side)	99.5%	99.5%

Table 6 illustrates the success rates obtained for measurements at points P1 and P2, considering noisy and noiseless signals. The high accuracy maintained by the proposed method for this new test system indicates its ability to be applied to different systems. Furthermore, the superimposition of noise on the signals for this test system had no impact on the method's performance since the scenarios in which the method failed were the same for tests with and without noise.

VIII. CONCLUSION

This paper presented a performance review of the main state-of-the-art fault classifiers when applied to IBR interconnection lines and proposed an innovative time-domain fault classification method. For these studies, PSCAD software was employed to model a system with a typical topology for connecting IBRs to the primary grid. Extensive simulations of fault scenarios on the interconnection line are performed, covering variations in fault type, location, inception angle, resistance, grid short-circuit levels, and IBR configurations.

Firstly, it was proven that the classifiers with a decision process based exclusively on voltage signals performed more

satisfactorily when considering measurements on the IBR side (point P1 of the test system), especially VMA-C, which can be applied to all fault types and provided the highest success rates among the state-of-the-art methods. In this context, the main IBR particularities that compromised the performance of each evaluated method were discussed and demonstrated.

Next, the voltage-based state-of-the-art classifiers' response in time was analyzed, revealing that their dependence on the phasor estimation process and the influence of IBR behavior resulted in more than 40 ms response times, depending on the method and fault type.

Thus, based on the performance analysis of the existing methods and identifying possibilities for improvement, a high-sensitivity fault classification method based on time-domain voltage signals was presented. The method is free of hard thresholds and outperforms the existing ones.

Furthermore, the generalizability of all the classifiers for applications in conventional generator terminals was also assessed. In summary, significant improvements were observed in the performance of the current signal-based methods, along with a considerable drop in the success rates of the VM-PS and VMA-C methods. The proposed method, in contrast, maintained the highest success rates, standing out among all the classifiers for its short response time, applicability to all fault types, and robustness to operate in systems with IBRs or conventional generators.

Finally, a second test system was evaluated to explore the ability of the proposed fault classification methodology to be applied to other systems, along with the influence of signal noise on its performance. The proposed method demonstrates high accuracy for this new test system, highlighting its potential for application across various systems. Additionally, the introduction of noise into the signals did not affect the proposed method's performance.

REFERENCES

[1] IEEE-PES, *Impact of Inverter Based Generation on Bulk Power System Dynamics and Short-Circuit Performance*, Standard PES-TR68, 2018.

[2] R. Chowdhury and N. Fischer, "Transmission line protection for systems with inverter-based resources—Part I: Problems," *IEEE Trans. Power Del.*, vol. 36, no. 4, pp. 2416–2425, Aug. 2021.

[3] M. J. B. B. Davi, M. Oleskovicz, F. V. Lopes, and D. C. Jorge, "A case study-based review of the impacts of inverter-interfaced wind power plants on distance protections," *J. Control, Autom. Electr. Syst.*, vol. 34, no. 3, pp. 599–608, Jun. 2023.

[4] B. Kasztenny, "Distance elements for line protection applications near unconventional sources," Schweitzer Eng. Lab., Pullman, WA, USA, Tech. Rep., 2021.

[5] A. Hooshyar and R. Iravani, "A new directional element for microgrid protection," *IEEE Trans. Smart Grid*, vol. 9, no. 6, pp. 6862–6876, Nov. 2018.

[6] A. Banaiemoqadam, A. Hooshyar, and M. A. Azzouz, "A control-based solution for distance protection of lines connected to converter-interfaced sources during asymmetrical faults," *IEEE Trans. Power Del.*, vol. 35, no. 3, pp. 1455–1466, Jun. 2020.

[7] *IEEE Standard for Interconnection and Interoperability of Inverter-Based Resources (IBRS) Interconnecting With Associated Transmission Electric Power Systems*, Standard IEEE 2800, 2022, pp. 1–180.

[8] R. Chowdhury and N. Fischer, "Transmission line protection for systems with inverter-based resources—Part II: Solutions," *IEEE Trans. Power Del.*, vol. 36, no. 4, pp. 2426–2433, Aug. 2021.

[9] D. Gupta, O. P. Mahela, and S. Ali, "Current based transmission line protection algorithm using signal processing techniques," in *Proc. IEEE Int. Students' Conf. Electrical, Electronics Comput. Sci. (SCEECS)*, Feb. 2020, pp. 1–6.

[10] A. Kumar, Aditya, S. Raj, A. K. Swarnkar, K. Barnwal, and S. Debnath, "A single ended wavelet based fault classification scheme in transmission line," in *Proc. IEEE Appl. Signal Process. Conf. (ASPCON)*, Dec. 2018, pp. 29–33.

[11] V. P. Goli and S. Das, "A transient current based DG interconnected transmission system protection scheme using wavelet analysis," in *Proc. IEEE Kansas Power Energy Conf. (KPEC)*, Jul. 2020, pp. 1–6.

[12] F. Lopes, J. Costa, T. Honorato, R. Toledo, L. Gama, P. Pereira, G. Salge, and M. Davi, "Busbar capacitance modeling effects during relay testing procedures for transmission lines interconnecting wind power plants," *J. Control, Autom. Electr. Syst.*, vol. 33, no. 2, pp. 541–549, Apr. 2022.

[13] F. V. Lopes, M. J. B. B. Davi, and M. Oleskovicz, "Assessment of traveling wave-based functions in inverter-based resource interconnecting lines," *Electric Power Syst. Res.*, vol. 223, Oct. 2023, Art. no. 109578.

[14] H.-H. Chang, N. V. Linh, and W.-J. Lee, "A novel nonintrusive fault identification for power transmission networks using power-spectrum-based hyperbolic S-transform—Part I: Fault classification," *IEEE Trans. Ind. Appl.*, vol. 54, no. 6, pp. 5700–5710, Nov. 2018.

[15] M. Coban and S. S. Tezcan, "Detection and classification of short-circuit faults on a transmission line using current signal," *Bull. Polish Acad. Sci. Tech. Sci.*, vol. 69, Jun. 2021, Art. no. 137630.

[16] M. M. Taheri, H. Seyedi, and B. Mohammadi-Ivatloo, "A decision-tree based relaying scheme for fault classification in transmission lines using magnitude of differential power," *IET Gener., Transmiss. Distrib.*, vol. 11, pp. 1–30, Mar. 2017.

[17] P. Krishnamurthy, S. Thangavel, R. Dhanalakshmi, and S. N. Khushi, "Fault classification in power system with inverter-interfaced renewable energy resources using machine learning," *J. Control, Autom. Electr. Syst.*, vol. 35, no. 6, pp. 1019–1038, Dec. 2024.

[18] S. Etukuri, M. Siva, and B. R. K. Varma, "Enhanced fault classification in inverter-fed transmission lines using deep learning," *Eng. Res. Exp.*, vol. 6, no. 4, Dec. 2024, Art. no. 045302.

[19] K. Al Kharusi, A. El Haffar, and M. Mesbah, "Fault detection and classification in transmission lines connected to inverter-based generators using machine learning," *Energies*, vol. 15, no. 15, p. 5475, Jul. 2022.

[20] M. J. B. B. Davi, M. Oleskovicz, and F. V. Lopes, "Exploring the potential of a machine learning-based methodology for fault classification in inverter-based resource interconnection lines," *Electric Power Syst. Res.*, vol. 223, Oct. 2023, Art. no. 109532.

[21] D. Costello and K. Zimmerman, "Determining the faulted phase," in *Proc. 63rd Annu. Conf. Protective Relay Engineers*, Mar. 2010, pp. 1–20.

[22] B. Kasztenny, B. Campbell, and J. Mazereeuw, "Phase selection for single-pole tripping—Weak infeed conditions and cross-country faults," in *Proc. 27th Annual Western Protective Relay Conf.*, Oct. 2000, pp. 1–19.

[23] D. V. Coury, M. Oleskovicz, and R. Giovanini, *Digital Protection of Electrical Power Systems: From Electromechanical Relays to Intelligent Microprocessors*. São Carlos, Brazil: Univ. Sao Paulo, 2011, p. 378.

[24] G. Benmouyal and J. Mahseredjian, "A combined directional and faulted phase selector element based on incremental quantities," *IEEE Trans. Power Del.*, vol. 16, no. 4, pp. 478–484, Oct. 2001.

[25] E. M. Carrasco, M. P. C. Moreno, M. T. V. Martínez, and S. B. Vicente, "Improved faulted phase selection algorithm for distance protection under high penetration of renewable energies," *Energies*, vol. 13, no. 3, p. 558, Jan. 2020.

[26] A. A. Aboelnaga and M. A. Azzouz, "Reliable phase selection method for transmission systems based on relative angles between sequence voltages," *J. Modern Power Syst. Clean Energy*, vol. 12, no. 5, pp. 1431–1444, 2024.

[27] V. Chakrapani and I. Voloh, "Impact of renewable generation resouce on the distance protection and solutions," in *Proc. 16th Int. Conf. Develop. Power Syst. Protection (DPSP)*, Mar. 2022, pp. 238–243.

[28] M. M. Mobashsher, A. A. Abdoos, S. M. Hosseini, S. M. Hashemi, and M. Sanaye-Pasand, "A new fault type classification method in the presence of inverter-based resources," *Int. J. Electr. Power Energy Syst.*, vol. 147, May 2023, Art. no. 108793.

[29] A. Hooshyar, E. F. El-Saadany, and M. Sanaye-Pasand, "Fault type classification in microgrids including photovoltaic DGs," *IEEE Trans. Smart Grid*, vol. 7, no. 5, pp. 2218–2229, Sep. 2016.

[30] S. Paladhi and A. K. Pradhan, "Adaptive fault type classification for transmission network connecting converter-interfaced renewable plants," *IEEE Syst. J.*, vol. 15, no. 3, pp. 4025–4036, Sep. 2021.
[31] Y. U. Khan, O. D. Naidu, and A. K. Pradhan, "A fault classification method for power transmission line connected to converter interfaced renewable power plants," in *Proc. 22nd Nat. Power Syst. Conf. (NPSC)*, Dec. 2022, pp. 148–153.
[32] A. Morched, B. Gustavsen, and M. Tartibi, "A universal model for accurate calculation of electromagnetic transients on overhead lines and underground cables," *IEEE Trans. Power Del.*, vol. 14, no. 3, pp. 1032–1038, Jul. 1999.
[33] B. Gustavsen, G. Irwin, R. Mangelrod, D. Brandt, and K. Kent, "Transmission line models for the simulation of interaction phenomena between parallel AC and DC overhead lines," in *Proc. IPST*, 1999, pp. 61–67.
[34] R. Gagnon, G. Turmel, C. Larose, J. Brochu, G. Sybille, and M. Fecteau, "Large-scale real-time simulation of wind power plants into hydro-quebec power system," in *Proc. 9th Int. Workshop Large-Scale Integr. Wind Power Power Syst. Transmiss. Networks Offshore Wind Power Plants*, 2010, pp. 18–19.
[35] N. W. Miller, J. J. Sanchez-Gasca, W. W. Price, and R. W. Delmerico, "Dynamic modeling of GE 1.5 and 3.6 MW wind turbine-generators for stability simulations," in *Proc. IEEE Power Eng. Soc. Gen. Meeting*, vol. 3, Jul. 2003, pp. 1977–1983.
[36] O. Tremblay, R. Gagnon, and M. Fecteau, "Real-time simulation of a fully detailed type-iv wind turbine," in *Proc. IPST*, Jul. 2013, pp. 18–20.
[37] T. Kauffmann, U. Karaagac, I. Kocar, S. Jensen, E. Farantatos, A. Haddadi, and J. Mahseredjian, "Short-circuit model for type-IV wind turbine generators with decoupled sequence control," *IEEE Trans. Power Del.*, vol. 34, no. 5, pp. 1998–2007, Oct. 2019.
[38] A. Guzmán, J. Roberts, and D. Hou, "New ground directional elements operate reliably for changing system conditions," in *Proc. 50th Annu. Conf. Prot. Relay Eng.*, 1997, pp. 1–27.
[39] A. Guzmán, M. V. Mynam, V. Skendzic, and J. L. Eternod, "Directional elements—How fast can they be?" in *Proc. 44th Annu. Western Protective Relay Conf.*, 2017, pp. 1–22.
[40] A. Hooshyar, M. A. Azzouz, and E. F. El-Saadany, "Distance protection of lines emanating from full-scale converter-interfaced renewable energy power plants—Part I: Problem statement," *IEEE Trans. Power Del.*, vol. 30, no. 4, pp. 1770–1780, Aug. 2015.

MOISÉS J. B. B. DAVI received the B.Sc. degree in electrical engineering and the M.Sc. degree in technological innovation from the Federal University of Triangulo Mineiro, in 2014 and 2021, respectively, and the Ph.D. degree in electrical engineering from São Carlos School of Engineering (EESC), University of São Paulo (USP), Brazil, in 2025. He has extensive experience in power system protection, IED commissioning, electromagnetic transient simulation and analysis, and oscillography interpretation. His research interests include protective relaying, power system transients, advanced power system modeling, fault location techniques, and the control and protection of renewable energy systems.

MARIO OLESKOVICZ (Member, IEEE) received the degree in electrical engineering from the Federal University of Santa Catarina (UFSC), Brazil, in 1995, and the M.Sc. and Ph.D. degrees in electrical engineering from São Carlos Engineering School (EESC), University of São Paulo (USP), Brazil, in 1997 and 2001, respectively. He is an Assistant Professor with the Department of Electrical and Computer Engineering, EESC. He works in the electrical engineering area, focusing on power systems (generation, transmission, distribution, and microgrids), power quality, and power system digital protection.

FELIPE V. LOPES (Senior Member, IEEE) was born in Brazil, in 1985. He is currently a Professor with the Graduate Program on Renewable Energies, Department of Electrical Engineering, Federal University of Paraíba (UFPB), Brazil. In recent years, he has conducted various researches on power system transients, electrical grid modeling, fault location, and protection solutions for power networks with conventional and unconventional sources. He was recognized as a Research Productivity Scholar by the Brazilian Council for Scientific and Technological Development (CNPq). Since 2017, he has been involved with activities of the CIGRE B5 Study Committee, Brazil. He is an Associate Editor of IEEE TRANSACTIONS ON POWER DELIVERY and *Power Engineering Letters*.